EVOLUTIONARY BIOLOGY

Ediacaran metazoan reveals lophotrochozoan affinity and deepens root of Cambrian Explosion

A. J. Shore[1]*, R. A. Wood[1], I. B. Butler[1], A. Yu. Zhuravlev[2], S. McMahon[1,3], A. Curtis[1], F. T. Bowyer[1†]

Through exceptional preservation, we establish a phylogenetic connection between Ediacaran and Cambrian metazoans. We describe the first three-dimensional, pyritized soft tissue in *Namacalathus* from the Ediacaran Nama Group, Namibia, which follows the underlying form of a stalked, cup-shaped, calcitic skeleton, with six radially arranged lobes projecting into an apical opening and lateral lumens. A thick body wall and probable J-shaped gut are present within the cup, and the middle layer of the often-spinose skeleton and skeletal pores are selectively pyritized, supporting an organic-rich composition and tripartite construction with possible sensory punctae. These features suggest a total group lophotrochozoan affinity. These morphological data support molecular phylogenies and demonstrates that the origin of modern lophotrochozoan phyla, and their ability to biomineralize, had deep roots in the Ediacaran.

INTRODUCTION

Exceptional preservation of fossils from the Ediacaran-Cambrian, ca. 570 to 500 million years (Ma) ago, provides great insight into the first radiation of metazoans. While the oldest putative skeletal metazoans known are from the terminal Ediacaran, the general absence of both definitive skeletal characteristics and soft-tissue preservation has precluded clear assignment of affinity and, hence, an understanding of the origin of major metazoan groups. Here, we describe the first, three-dimensional, pyritized preservation of soft tissue in the Ediacaran skeletal metazoan *Namacalathus hermanastes*, from the Nama Group, Namibia, where new features support a bilaterian, lophotrochozoan affinity. In so doing, we also establish a strong evolutionary link between terminal Ediacaran and early Cambrian taxa.

Namacalathus is a sessile, benthic skeletal organism with a widespread distribution known from diverse carbonate settings, including thrombolite reefs and shallow lagoons, ca. 550 to 540 Ma ago. *Namacalathus* has a goblet-like skeletal morphology formed by a hollow stalk expanding into a calyx from ca. 3 to 35 mm in diameter with an apical central opening and five to seven, but generally six, lateral lumens (*1*–*3*). Spines are present on the outer surface of the stem and cup in some individuals (*2*), and adjacent individuals have been found with shared cavities, interpreted as representing potential bilateral, asexual, external budding (*3*). Present skeletal mineralogy is generally low-Mg calcite, but the original mineralogy may have been either Mg calcite or aragonite (*1*,*4*). Preserved plastic deformation implies that skeletal walls were flexible and, therefore, organic rich (*1*). Skeletal microstructure has been described as a diagenetic, tufa-like cement (*5*), but well-preserved specimens display foliated outer and inner skeletal layers, with a middle layer inferred to have been organic rich (*3*).

Namacalathus has been proposed to be a cnidarian because of its hexaradial symmetry and a goblet-like morphology, as found in some hydrozoan polyps, scyphozoan scyphistomae, and stauromedusae (*1*). Others have suggested a protozoan affinity because of the absence of accretionary growth (*6*) or a total group lophophorate based on foliated skeletal microstructure and bilateral budding (*3*). Recently, a stem group ctenophore affinity has been proposed on the basis of phylogenetic analyses and a general morphological similarity to sessile, Cambrian skeletonized "dinomischids" and scleroctenophores (*7*).

RESULTS

Here, we report exceptionally preserved *Namacalathus* individuals found within the uppermost Upper Omkyk Member of the Nama Group, Namibia, from a low-energy, very shallow, dominantly carbonate, inner ramp setting, just below an ash bed dated at 547.32 ± 0.65 Ma old (see fig. S1) (*8*). *Namacalathus* individuals range from 4 to 12 mm in diameter, although many are partially covered with sediment and are preserved as reddish brown to yellow (oxyhydr) oxide minerals, FeOx ["FeOx" here denotes unspecified iron (oxyhydr) oxide] resulting from oxidation of pyrite (FeS_2), or as raised gray limestone casts that sometimes reveal weathered sections through the calcified skeleton (Fig. 1 and figs. S2A and S3). Seventy-three individuals (numbered 1 to 73) are found on a bedding plane sample, some with stalks (fig. S2, A and D), with 29% preserved upright in inferred growth position, 48% slightly toppled, and 23% of undetermined orientation (fig. S3). The host lithology is finely laminated micrite that grades from a mud-rich packstone with some silt-grade quartz and recrystallized bioclasts, often with a stylolitic contact (fig. S2C). *Namacalathus* individuals are immediately overlain by a thin (<1 mm) micritic carbonate with silt-grade, angular lithic fragments of quartz, albite, clays, and phosphatic minerals (figs. S4 and S5).

The best-preserved individuals show a raised pin cushion–like form, which surrounds the central, apical, opening. The central apical opening ranges from 1.3 to 12.3 mm (n = 37, mean = 3.6 mm) in diameter and can either be circular (Fig. 1, E and F, and fig. S3, K to N) or show five to seven, but generally six, isoclinal folds that radiate outward (Fig. 1, A to D and F, and fig. S3, A to J, P, and Q). Fold height ranges from 0.18 to 2.78 mm and width ranges from 0.43 to 4.66 mm (table S1). Both types of opening are preserved either as an FeOx crust (Fig. 1, A to D and F, and fig. S3, A to G and M to Q) or as casts of limestone (Fig. 1, E and I, and fig. S3, H to L and W to X). In cups where the central opening and lumens are visible, central opening folds oppose folds across the lumens (Fig. 1D). Full lumens are

[1]School of GeoSciences, University of Edinburgh, James Hutton Road, Edinburgh EH9 3FE, UK. [2]Department of Biological Evolution, Faculty of Biology, Lomonosov Moscow State University, Leninskie Gory, Moscow 119991, Russia. [3]UK Centre for Astrobiology, School of Physics and Astronomy, University of Edinburgh, James Clerk Maxwell Building, Peter Guthrie Tait Road, Edinburgh EH9 3FD, UK.
*Corresponding author. Email: amy.shore@ed.ac.uk
†Present address: School of Earth and Environment, University of Leeds, Leeds LS2 9JT, UK.

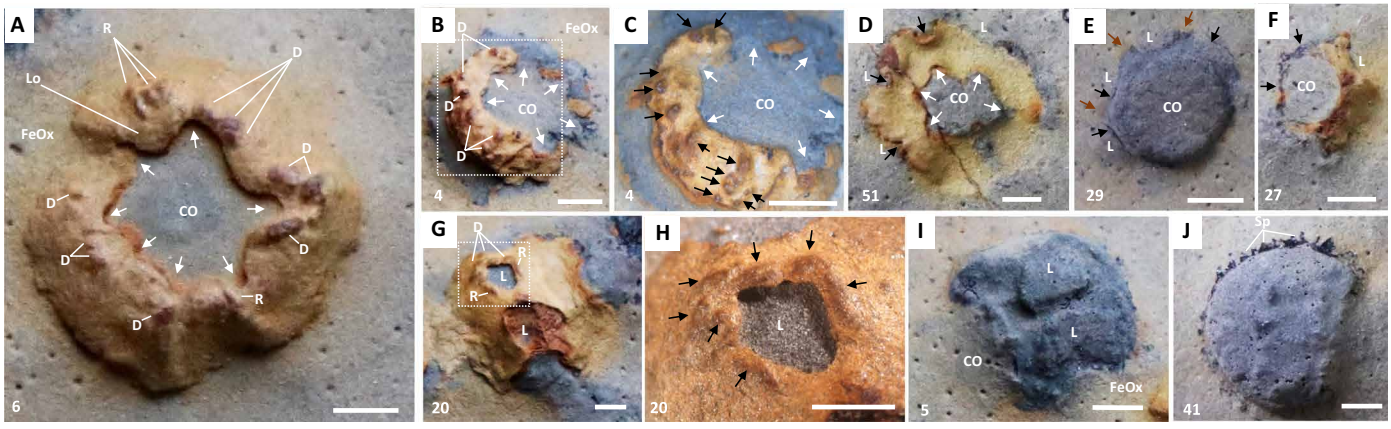

Fig. 1. *N. hermanastes*, Nama Group, Namibia. Museum No. F1547, Museum of the Geological Survey of Namibia. For numbered individuals, see fig. S2A. Scale bars, 2 mm. (**A** to **D**) Upright *Namacalathus* cup showing the central opening (CO) with folds (white arrows). Ridges (R) and domes (D) are present around the CO, with intervening pillow-like lobes (Lo), and iron (oxyhydr)oxide staining (FeOx) of sediment around fossil. (B) Folds (arrowed) around the CO and associated D. (C) Inset of (B), showing radiating D (black arrows) and folds (white arrows) around the CO. (D) Upright view showing folds (white arrows) around the central CO and lumens (L) with opposing folds (black arrows). (**E**) Cast preservation, with the CO and top of three L with calcite skeleton (black arrows). Sediments between lumens stained with FeOx (brown arrows). (**F**) CO and L preserved in FeOx, with calcite skeleton beneath (black arrows). (**G**) Toppled *Namacalathus* cup with R and D around L. (**H**) Inset of (G), showing domes and ridges (black arrows) around L. (**I**) Cast of toppled *Namacalathus* with L and CO. (**J**) Toppled *Namacalathus* with spines (Sp).

similarly observed either as FeOx crusts (Fig. 1, G and H, and fig. S3, P to U) or as casts (Fig. 1I and fig. S3, V to Y). Lumen height is smaller when preserved by FeOx (mean = 1.59 mm) compared to limestone casts (mean = 2.34 mm), but preservation style does not notably influence lumen width (mean = 1.8 mm; fig. S6B). Small (0.33 to 1.27 mm; table S2), domal, or elongate ridge-like swellings are present around the edges of the central opening and lumens (Fig. 1, A to C, G, and H, and fig. S7), concentrated at the apex of folds around the apical opening (Fig. 1A and figs. S3, A and C, and S8, A and B) or parallel to the edges of the lumen in one specimen (Fig. 1, G and H, and figs. S3R and S7, C and D), or as pairs that radiate from the apical opening to the lumens (Fig. 1, B and C, and fig. S3, C, D, and P). The calcitic skeleton is also preserved (Fig. 1, E, F, and J, and fig. S3, Q, Z, and A*ii* to A*v*), revealing robust, radiating spines of up to 0.4 mm in length and width where the FeOx crust has not been preserved (Fig. 1J and fig. S3, Z to A*v*).

X-ray micro–computed tomographic (μCT) imaging of two individuals (nos. 4 and 32) shows that pyritization reveals the presence of soft tissue as well as a cup-shaped calcite skeleton without a stalk below the bedding plane surface (Fig. 2 and fig. S8). Both visual inspection of the fossils (Fig. 1) and μCT images reveal the uppermost soft tissue to be present as six radially arranged lobes separated by the folds that project into the central opening and into the top of the lumens (Fig. 2). A cluster of helically coiled large bacteria, possibly *Obruchevella*, known mostly from Neoproterozoic and Cambrian successions (*9*), is also selectively pyritized outside the *Namacalathus* cup (Fig. 2, C, F to H, and K to M).

Polished serial sections through *Namacalathus* (no. 32) confirm the presence of an internal calcite skeleton with selective pyritization, with the overlying soft-tissue lobes preserved by framboidal pyrite, the vast majority of which is oxidized to FeOx and is thus referred to here as FeOx framboids that are pseudomorphs after pyrite (Figs. 2, D, I, and N, and 3, and figs. S9 and S10). Backscatter scanning electron microscopy (SEM) images also distinguish between the selectively pyritized calcitic skeleton and lobes preserved wholly via pyritization (Fig. 3A and figs. S11 and S12). Horizontal calcitic skeletal flanges are present that extend outward up to 950 μm from the central opening (Figs. 2N, 3A, and 4C), which abut with straight edges against the pyritized lobes as revealed by cathodoluminescence (CL) imaging (Fig. 4D). FeOx staining of up to 0.5 mm thick is also apparent within the cup adjacent to the inner wall (Figs. 2, D, I, and N; 3A; and 4B), which extends into the lumens (Fig. 2N and fig. S10, B and C), and also in patches of up to 0.1 mm thick on the outer wall (Fig. 2I). Thin, FeOx-rich channels 50 to 300 μm wide are present that extend orthogonally through the entire wall thickness, often passing through the central parts of spines (Figs. 3, A, E, and F, and 4, E and F). Slits also appear parallel to the skeletal wall (Fig. 4H), or between spines (Fig. 4I), and may bifurcate (Fig. 4I). These slits extend to at least 450 μm in depth (figs. S10 and S13). FeOx staining is notable on both the outer and inner walls where the channels terminate (Figs. 2, D, I, and N; 3, E and F; and 4, E and G to I). CL imaging shows the skeleton to be composed of poorly zoned, dominantly dull luminescent, blocky neomorphic sparry calcite (Fig. 4, F and R), where crystals differing in orientation are present on either side of the pyritized pores (Fig. 4F).

A tube-like structure, often defined by a central area of framboidal FeOx and an outer area of nonzoned, dark dull luminescent, sparry calcite (also present as a later-stage cement infill within the carbonate sediment), is found within three of four *Namacalathus* cups analyzed and can be distinguished in polished serial sections, as well as imaging via CL and backscatter SEM (Figs. 2, D, I, and N; 3, A and D; and 4, L and M; and figs. S4, S9, S13, and S14) and μCT (Fig. 2, E, G, H, J to M, and O). This structure has an elliptical cross section of up to 400 μm in diameter and may connect with a thin layer of FeOx 100 to 400 μm thick draped across the central opening of the cup (Figs. 2, D, I, and N; 3D; and 4, N and O). The tube then descends into the cup moving toward the inner wall, inflating to a circular section up to 600 μm, and then curves to form a J-shaped structure within the cup (Fig. 2, E, J, and O), sometimes decreasing in width to lastly disappear without attachment (fig. S12).

FeOx framboids are abundant in both the soft tissue (Fig. 3C and figs. S11 and S12) and skeleton (Fig. 3J and figs. S5 and S12). There

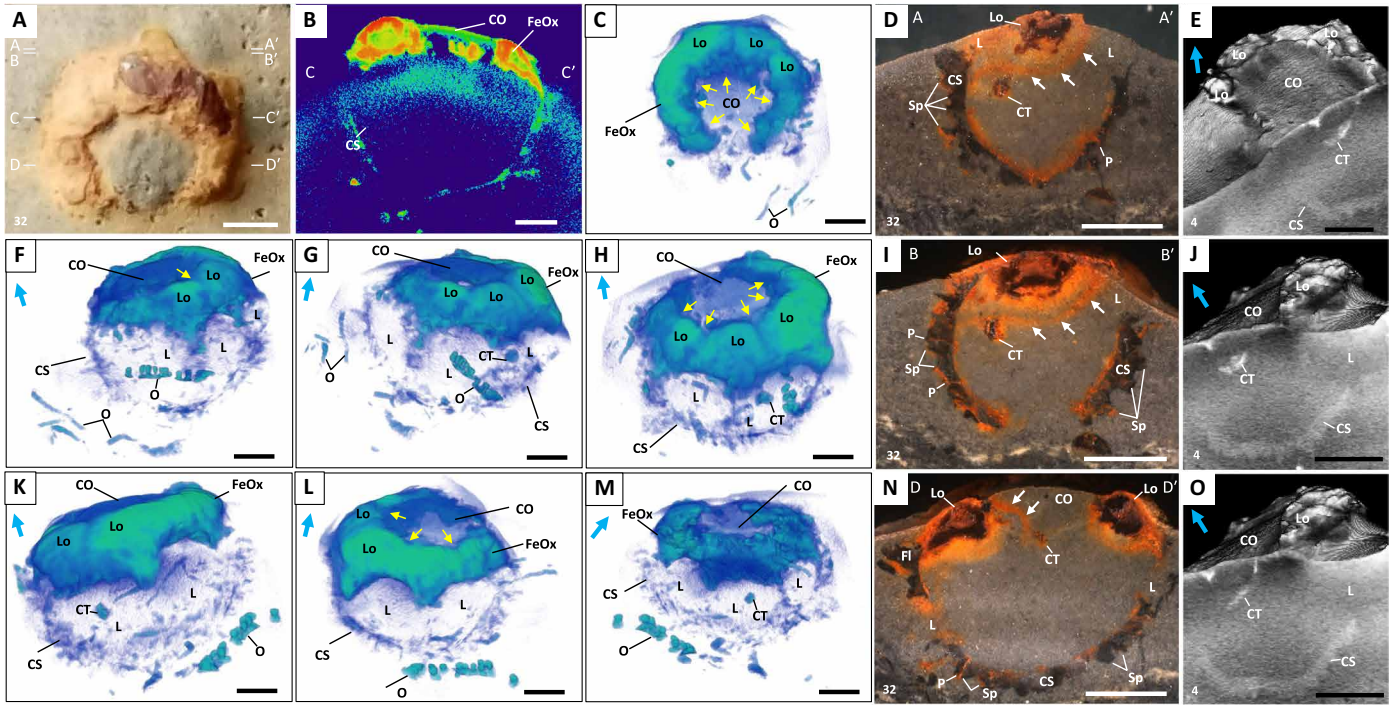

Fig. 2. X-ray μCT reconstruction of *N. hermanastes*. Museum No. F1547, Museum of the Geological Survey of Namibia. (A) to (D), (F) to (I), and (K) to (N), no. 32, and (E), (J), and (O), no. 4 showing the CO surrounded by FeOx (green-blue), showing Lo, L, and folds (yellow arrows). The calcite skeleton (CS; blue) is preserved below the bedding surface and outlines the L. CT, central tube; scale bars, 2 mm. (**A**) Plain view of *Namacalathus* cup. (**B**) False-color μCT slice of core (C to C′ of A). (**C**, **F** to **H**, and **K** to **M**) Reconstruction of *Namacalathus* cup rotated from the central axis. O, large bacterium, possible *Obruchevella*. (**D**, **I**, and **N**) Photomicrographs of successive longitudinal surfaces during serial sectioning (A and A′, B and B′, and D and D′ of A), with arrows tracing the membrane across the CO. (**E**, **J**, and **O**) Rendered three-dimensional model with grayscale CT sections, highlighting Lo, CS, and CT. Sp, spine; P, pore; CT, central structure; Fl, flange; white arrows, iron oxide concentration within the cup; blue arrows, way up.

are no framboids in the wider sediment. The neomorphic sparry calcite skeleton of *Namacalathus* also contains extensive FeOx framboids. These often occur within a well-defined, straight-edged middle layer (Fig. 3G), where pyritization extends to almost the full width of the skeleton in the uppermost parts of the cup, thinning toward the base of the cup where the calcitized outer and inner skeletal layers thicken (Fig. 3, G and H). Thin accumulations of FeOx framboids also occur in patches along the inner and outer skeletal surfaces and additionally pick out inverted V-shapes within the calcitic parts of the skeleton (Fig. 3, G and J). CL imaging shows zoned calcite cements growing around uncompacted sediment, which project into the neomorphic calcite skeleton of *Namacalathus* and other neomorphosed bioclastic grains (Fig. 4F). The dominant bright CL zone of the zoned calcite cements growing around uncompacted sediment coincides with visible FeOx staining near the upper parts of the cup (Fig. 4, C and D) and also with the thin layer of FeOx across the central opening (Figs. 2, D, I, and N, and 4, N and O). SEM images of this area confirm the presence of a line of framboidal FeOx (Fig. 3D).

Peloids are abundant in the area with visible iron staining, where the peloids are partially replaced by pyrite/FeOx (Fig. 3H). Likewise, sediment grains in the bed surface overlying the *Namacalathus* individuals are coated by pyrite/FeOx cements (Fig. 3I). Thus, CL imaging reveals three carbonate sediment types associated with the *Namacalathus* cups (Fig. 3C)—a bioclast-rich sediment infilling the bottom of cups (S1), a peloid-rich sediment with partial pyrite/FeOx replacement in the upper part of cups (S2), and an overlying lithic-rich sediment with pyrite/FeOx cements (S3) (Figs. 3, H and I, and 4R).

DISCUSSION

We therefore infer that early precipitation of both pyrite and calcite cements is responsible for this exceptional, three-dimensional preservation (*10*). This type of preservation occurs in sulfate-reducing environments with high concentrations of highly reactive iron but low or very localized availability of organic carbon available during early diagenesis, where pyrite precipitation is only associated with labile tissues and cellular structure is destroyed (*10*) and where the form of pyrite may reflect the relative susceptibility to decay of the original material (*11*,*12*). Pyrite framboid formation can occur within hours to days on organic matter under these conditions (*13*). We infer that framboidal pyrite formed very early and replaced both soft tissue and the inferred organic-rich parts of the skeleton. The occurrence of pyritized bacteria, here found alongside *Namacalathus*, is highly unusual in the fossil record and confirms that pyritization was rapid enough to replicate soft tissue.

The bright CL zone of early calcite cements associated with sediment within the upper part of cups (S2) is indicative of high-Mn and low-Fe pore water conditions (fig. S4). The sediment of S2 is also characterized by FeOx staining, which is inferred to derive from the oxidation of pyrite. This confirms the coincidence of both early

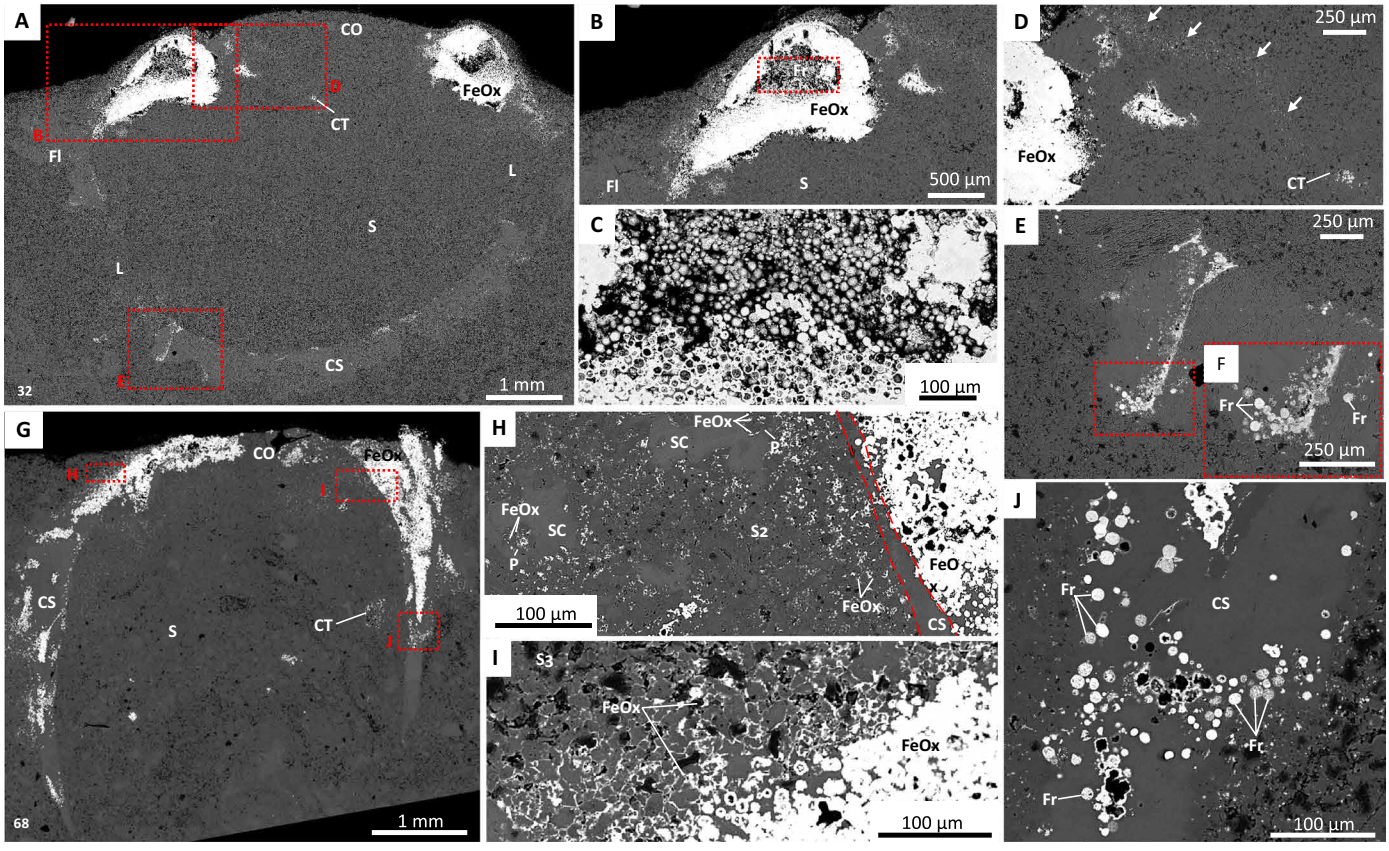

Fig. 3. Backscatter SEM images of *N. hermanastes*. Museum No. F1547, Museum of the Geological Survey of Namibia. (A) to (F), no. 32, slices D and D′ (Fig. 2N). (G) to (J), no. 68. (**A**) Scanning electron microscopy (SEM) image showing CS and FI with L, pyritized/FeOx soft tissue of lobes (FeOx) and CT, with S. (**B**) Inset of (A), soft-tissue lobe of *Namacalathus* at the bedding surface infilled by FeOx framboids (Fr). (**C**) Inset of (B), showing FeOx Fr. (**D**) Inset of (A), showing line of FeOx Fr (arrowed) across the CO, which attach to CT. (**E**) Inset of (A), spine with perpendicular pore infilled with FeOx Fr. (**F**) Inset of (E), showing FeOx Fr. (**G**) FeOx Fr within the central area of the skeleton and CT. (**H**) Inset of (G), showing the middle layer of FeOx Fr (FeOx) in CS widening toward the bedding surface, and S2 peloidal sediment with FeOx (arrowed) partially replacing peloids (P). SC, burial sparry calcite. (**I**) Inset of (G), FeOx cement around angular calcitic and lithic grains of S3. (**J**) Inset of (G), FeOx Fr within the CS.

pyrite and early calcite cementation. Early carbonate cement formation is known to be facilitated by cell walls, extracellular polymeric substances, organic matter degradation, and other metabolic or microbial processes where peloids may form [e.g., (*14*)]. Local dissolution around pyritized soft tissue, perhaps induced by limited oxidation of pyrite, led to the formation of molds that later became infilled with a burial calcite spar cement.

Similar three-dimensional preservation of soft tissues in pyrite is found in the terminal Ediacaran Gaojiashan Member of the Dengying Formation, China (*15*), the Early Cambrian Chengjiang and Guanshan Lagerstätten from China (*11*), the Lower Ordovician Fenxiang Formation (*16*), and the Lower Cretaceous Santana Formation (*12*), often created by rapid entombment via storms. In the Nama Group, the proximal, very shallow, low-energy environment provided both a fine-grained medium and sufficient calcium carbonate saturation to facilitate early cementation. The *Namacalathus* individuals may also have been rapidly buried, in life, by a thin incursion of terrestrially derived lithic-rich sediment, and the folds of the central apical opening may represent a contracted state. The folding is unlikely to be taphonomic as the number of folds appears to correlate with lumen number (Fig. 1D). Cloudinids in siliciclastic-dominated beds of the Wood Canyon Formation, Nevada, show more spatially restricted framboidal pyritization that preserves cylindrical internal structures recently interpreted as possible digestive tracts (*17*). Internal digestive tissue is otherwise completely unknown from the Ediacaran record although common in Cambrian Lagerstätten (*17*). In sum, the processes operating in this preservational setting have created a taphonomically unique Lagerstätte.

The pyrite-rich middle layer within the *Namacalathus* skeleton confirms the presence of a tripartite skeleton with an organic-rich central portion (*3*). FeOx framboids in thin layers within other parts of the skeleton also suggest the presence of thinner organic-rich layers, parallel to potential accretionary growth lines. The additional presence of framboids that traverse the wall, as well as neomorphic calcite of differing orientations on either side of the pores, suggests that these are primary biological features, such as pores piercing the walls and the longer channels penetrating the spines. The thickness of the pyritized middle layer increases toward the upper part of the skeletal cup, suggesting that this may have been the area of initial skeletogenesis in contact with other soft tissue. This middle layer may have formed an organic template upon which the outer and inner calcareous layers formed and, as such, was the area of active skeletal growth, as observed in modern corals and lophophorates [e.g., (*18*)]. The FeOx staining noted extensively within the cup and lumens, and in

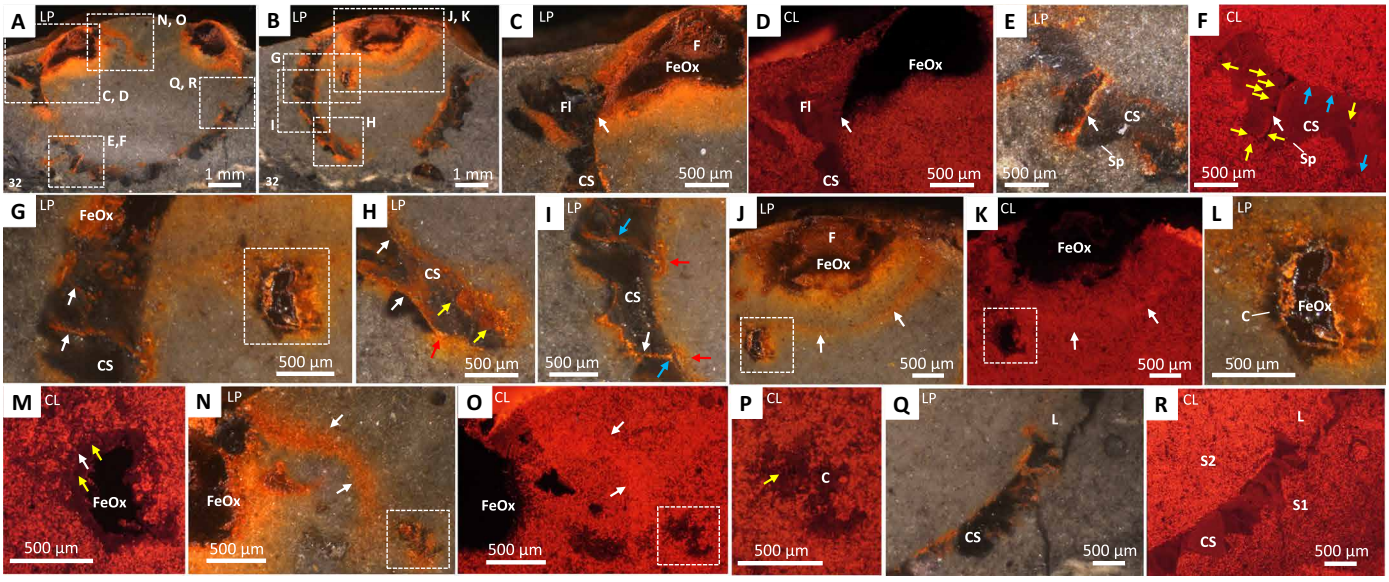

Fig. 4. Photomicrographs (LP) and CL images of *N. hermanastes*. Museum No. F1547, Museum of the Geological Survey of Namibia, no. 32. Longitudinal section highlighting features of the CS and FeOx. (**A**) Sections D and D′ (Fig. 2N) and (**B**) sections B and B′ (Fig. 2I) showing highlighted areas. (**C** and **D**) CS with a Fl overlain by FeOx (contact arrowed). (**E**) Pore (arrowed) along an Sp. (**F**) FeOx framboid-lined pore (F) (yellow arrow), forming a crystal boundary (white arrows). (**G**) Pores infilled with FeOx framboids (arrowed) and section of a central tubular structure (CT, boxed). (**H**) CS with FeOx staining parallel to (white arrows) and on the outer skeletal wall (yellow arrows). FeOx is concentrated where channels penetrate the outer wall of the cup (red arrow). (**I**) Channels with bifurcation (blue arrows) and with FeOx in areas between spines (white arrow). Concentrated FeOx located on the outer wall and where channels penetrate the inner wall of the cup (red arrows). (**J**) Lobe surrounded by FeOx staining (arrowed) connecting to CT (boxed). (**K**) FeOx staining coincident with bright luminescent calcite. (**L** and **M**) Section of CTS in (G) and (J), with sparry calcite (white arrow) surrounding F (yellow arrows). (**N** and **O**) FeOx staining of membrane (arrowed) coincident with brighter luminescence (arrowed), connecting to the CT. (**P**) Inset of (O), CT with calcite (C) with central F (yellow arrow). (**Q** and **R**) CS; lumen (L), with S1 and S2 sediments outside and inside the cup, respectively.

thinner patches inside and outside the cup, suggests the presence of soft tissue.

In sum, *Namacalathus* has a goblet-shaped calcareous skeleton with a hollow stalk and central opening, generally hexaradial symmetry with lateral facets bearing large lumens, a foliate microstructure with concordant columnar inflections and a middle organic-rich layer, and asexual reproduction expressed by bilateral budding (*1*,*3*). Soft tissue faithfully follows the internal skeleton, and the lumens do not have a localized, diagenetic, dissolution origin as previously suggested (*1*). In addition, we note the presence of folds formed between radially arranged lobes that extend from the central apical opening to lateral lumens, organic-rich pores, and channels within the skeletal wall; an internal, asymmetric, J-shaped tube-like structure, soft tissue adhering to the inner skeletal wall; an internal membrane abutting the central opening; and a thin organic-rich external covering. The tube-like structure is present in multiple specimens and has an apparent connection to the membrane across the aboral opening, suggesting a feeding function. Alternatively, this may represent a retractor muscle band but is more likely a gut or body cavity extension, potentially a partially preserved U-shaped gut. We note that the framboidal pyritic preservation of this putative gut is like that of the soft-tissue structure recently interpreted as a gut in cloudinids of the Wood Canyon Formation, Nevada (*17*). The small ridges and domes associated with the central opening and lumens could represent the base of tentacles; alternatively, they may have formed by the pyrite weathering process.

The pores or punctae may be homologous to those of similar size in brachiopods, extinct tommotiids, and microconchids, and to pseudopunctae in bryozoans, which house setae and other sensory structures (*19*–*21*). Punctae and channels connect the thin external and thick internal FeOx-rich layers, allowing interpretation as a mucopolysaccharide-protein periostracum and the body wall, respectively. The periostracum has a lobate pattern around the central opening, and these lobes could represent grooves where the tentacles were retracted. The variable constriction and scalloping of the central opening infers the presence of radially arranged, parietal diaphragm dilatator muscles. In some bryozoan groups, contraction of these muscles pulls the frontal membrane of the polyp inward with protrusion of the tentacle collar (*19*). The thin organic structure that traverses the apical opening of *Namacalathus* (Fig. 2, D, I, and N) can be interpreted as a frontal membrane, and so the position of the presumed gut below would correspond to the coelomic cavity following a lophophorate model. A retraction mechanism can also be inferred in *Namacalathus*, where muscle bundles may connect the frontal membrane and body wall (Fig. 2, D, I, and N).

This set of features, together with those seen in other specimens [bilateral budding and columnal inflections in the skeletal laminae (*3*)], excludes assignment of *Namacalathus* to protists, coralline algae, poriferans, cnidarians, and ctenophores (table S3). While hexaradial symmetry might favor an affinity within the Cnidaria, and some extinct Paleozoic corals have a foliated microstructure (*22*), the presence of skeletal columnar punctae, channels, a J- or U-shaped inferred gut, and a frontal membrane rather than a large, central, pharynx, as well as an absence of mesentery-like structures, does not support a cnidarian affinity.

Skeletal representatives of the Lophophorata, including stem and crown group brachiopods, bryozoans, and extinct microconchids, have very similar foliated microstructures with columnar inflections

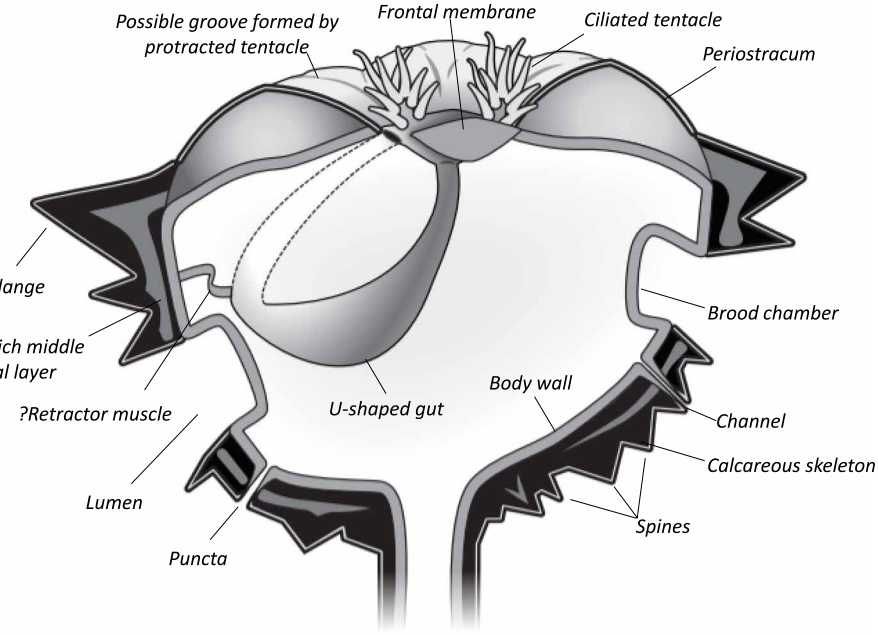

Fig. 5. Reconstruction of *N. hermanastes* as a total group lophotrochozoan.

in places extending into spines. A consensus tree for 54 lophotrochozoan taxa where *Namacalathus* occupies a basal position reveals that such "canaliculate" microstructure and "punctae" have multiple origins across the brachiozoan total group (*23*). The absence of any traces of a gastral cavity and the discovery of possible organic-rich punctae and channels within the skeletal walls further emphasize a similarity with the sensory porosity observed in lophophorates (brachiopods, tommotiids, and microconchids) (*21*,*24*), as does the presence of a possible J- or U-shaped gut. The generally six, large lateral lumens point to either a colonial organization for *Namacalathus* or a solitary organism in which lumens might correspond to brood chambers formed by external body wall invaginations, as found in bryozoans (*19*). Invaginations of the body wall are observed within the lumens in *Namacalathus* (fig. S10, B and C).

The confirmation of total group lophotrochozoans in the Ediacaran is supported by molecular phylogenies (*25*) and has implications for the earliest evolution of lophotrochozoans. The fossil record of biomineralized stem group lophotrochozoans is abundant from the early Cambrian onward where the possession of a calcareous skeleton or external sclerites likely represents the independent acquisition of skeletons of variable mineralogy in sessile, attached benthic fossil taxa, which have features shared with *Namacalathus*. These include tommotiids (*26*) and hyoliths, which were pedunculate and tentaculate organisms lacking a lophophore (*23*). Some goblet-shaped Cambrian forms that resemble *Namacalathus*, such as *Cotyledion tylodes* from the Chengjiang deposits, may represent stem lophophorates and also show an upper calyx and elongate stalk, with a central canal interpreted as an extension of the calycal cavity, a U-shaped gut with a mouth and aboral anus ringed by retractable marginal tentacles, and an outer surface covered by external sclerites, which may have been mineralized (*27*).

Cotyledion and some other Cambrian stalked fossils, namely, *Dinomischus* and *Siphusauctum*, have been compared with entoprocts (*27*–*29*). These fossils are relatively large (over 15 mm in height), while extant entoprocts are extremely small (less than 1 mm) and nonbiomineralized.

The Entoprocta are an enigmatic monophyletic acoelomate group that occupies a phylogenetically basal position among lophotrochozoans, close to molluscs (*30*). *Namacalathus* displays some notable similarities with the entoprocts, including the goblet-shaped overall morphology (a body divided into distinct stalk and calyx), hexaradial symmetry, the position of both mouth and anus within the presumable tentacle collar, and bilateral buds emerging from frontal area of the parental individual. Hence, we are now able to reconstruct *Namacalathus* as a total group lophotrochozoan, capable of asexual budding with an organic-rich, foliated calcareous skeleton and an open, apical J- or U-shaped gastric cavity within the apical opening potentially accommodating a retractable collar of tentacles and with brood chambers around the lumens (Fig. 5).

Sessile extant lophotrochozoan phyla such as annelids, molluscs, brachiopods, and phoronids have been suggested to have their origins in the earliest Cambrian small skeletal fauna [e.g., (*26*)], which are iconic representatives of the Cambrian Explosion. However, now, we can extend the origin of these modern lophotrochozoan phyla further back still into the terminal Ediacaran. In so doing, we establish a phylogenetic connection between Ediacaran and early Cambrian taxa, faunas that were previously thought distinct. We hence extend the roots of the Cambrian Explosion itself into the Ediacaran, where total group lophotrochozoans such as *Namacalathus* show a combination of features that became typical of both later lophophorates and representatives of the entoproctan-molluscan-annelidan branch.

MATERIALS AND METHODS

One float sample (237 mm by 194 mm by 33 mm) was collected from Zwartmodder Farm. A single-lens reflex camera and a binocular microscope were used to photograph and document each *Namacalathus*,

with ImageJ software used for the quantification of dimensions, such as lumen width and height.

The float sample was radiographed to determine whether individual *Namacalathus* cups had a density contrast with the surrounding sediment. Because of a high contrast, *Namacalathus* no. 32 was cored and underwent μCT scanning. Scanning was at 120 kV and 1500 projections (2 × 2 s exposure averaged) were collected and reconstructed by filtered back projection to 824 tomographic slices. The contrast was enhanced by applying the stretch histogram option in ImageJ, while not affecting the original data. Three-dimensional models of the scans were rendered using Avizo 9 software. Voxel size of reconstructions equates to 20.7 μm. The predefined color map "physics.icol" was applied to the model to aid in the visualization of the features of the fossil, but the false colors are not quantitatively correlated to any property of the object. The color thresholds of the color map were altered in Avizo (255-65535) to remove the background of the surrounding calcium carbonate sediment to produce a model of the whole individual. Scanning of *Namacalathus* cup no. 4 was also at 120 kV, using the same data acquisition parameters, and 633 tomographic slices were reconstructed. The model was rendered using Avizo 9, with a voxel size of 23 μm, using the predefined color map "greyscale.icol" as the low contrast of the scan did not lend itself to be rendered in false color.

Namacalathus no. 32 was then cut into three sections to observe the internal structure of the *Namacalathus* cup (fig. S9). These sections were finely polished and imaged using binocular microscopy and CL (fig. S10). One of the slices underwent serial sectioning at 26-μm increments, which were also imaged through binocular microscopy and CL.

Two highly polished thin sections were made of the slab to describe the lithology using petrographic microscopy. Three highly polished, uncovered thick sections (200 to 2000 μm) were cut from transverse sections of *Namacalathus* no. 68 for backscatter electron imaging and EDX analysis.

Two samples (nos. 66 and 68) were serially sectioned and highly polished at 1-mm and 500-μm increments, respectively, to understand the distribution of iron oxide and its relationship to the calcitic skeleton using light microscopy and CL imaging. Serial sectioning at 1 mm of a core plug containing *Namacalathus* no. 66 allowed us to observe the relationship between the iron oxide and the calcite skeleton. A CanoScan LiDE 210 flatbed scanner was used to scan each section (4000 dots per inch for both sections).

SUPPLEMENTARY MATERIALS

Supplementary material for this article is available at http://advances.sciencemag.org/cgi/content/full/7/1/eabf2933/DC1

REFERENCES AND NOTES

1. J. P. Grotzinger, W. A. Watters, A. H. Knoll, Calcified metazoans in thrombolite-stromatolite reefs of the terminal Proterozoic Nama Group, Namibia. *Paleobiology* **26**, 334–359 (2000).
2. H. J. Hofmann, E. W. Mountjoy, *Namacalathus-Cloudina* assemblage in Neoproterozoic Miette Group (Byng Formation), British Columbia: Canada's oldest shelly fossils. *Geology* **29**, 1091–1094 (2001).
3. A. Y. Zhuravlev, R. A. Wood, A. M. Penny, Ediacaran skeletal metazoan interpreted as a lophophorate. *Proc. R. Soc. B Biol. Sci.* **282**, 20151860 (2015).
4. S. B. Pruss, C. L. Blättler, F. A. Macdonald, J. A. Higgins, Calcium isotope evidence that the earliest metazoan biomineralizers formed aragonite shells. *Geology* **46**, 763–766 (2018).
5. M. D. Brasier, J. B. Antcliffe, R. H. T. Callow, in *Taphonomy: Process and Bias Through Time*, P. A. Allison, D. J. Bottjer, Eds. (Topics in Geobiology, 2011), vol. 32, pp. 519–567.
6. A. Seilacher, D. Grazhdankin, A. Legouta, Ediacaran biota: The dawn of animal life in the shadow of giant protists. *Paleont. Res.* **7**, 43–54 (2003).
7. Y. Zhao, J. Vinther, L. A. Parry, F. Wei, E. Green, D. Pisani, X. Hou, G. D. Edgecombe, P. Cong, Cambrian sessile, suspension feeding stem-group ctenophores and evolution of the comb jelly body plan. *Current Biol.* **29**, 1112–1125.e2 (2019).
8. S. A. Bowring, J. P. Grotzinger, D. J. Condon, J. Ramezani, M. J. Newall, P. A. Allen, Geochronologic constraints on the chronostratigraphic framework of the Neoproterozoic Huqf Supergroup, Sultanate of Oman. *Am. J. Sci.* **307**, 1097–1145 (2007).
9. A. H. Knoll, The early evolution of eukaryotes: A geological perspective. *Science* **256**, 622–627 (1992).
10. N. J. Butterfield, Exceptional fossil preservation and the Cambrian explosion. *Integr. Compar. Biol.* **43**, 166–177 (2003).
11. S. E. Gabbott, H. Xian-Guang, M. J. Norry, D. J. Siveter, Preservation of Early Cambrian animals of the Chengjiang biota. *Geology* **32**, 901–904 (2004).
12. G. L. Osés, S. Petri, C. G. Voltani, G. M. E. M. Prado, D. Galante, M. A. Rizzutto, I. D. Rudnitzki, E. P. da Silva, F. Rodrigues, E. C. Rangel, P. A. Sucerquia, M. L. A. F. Pacheco, Deciphering pyritization-kerogenization gradient for fish soft-tissue preservation. *Sci. Rep.* **7**, 1468 (2017).
13. D. Rickard, How long does it take a pyrite framboid to form? *Earth Planet. Sci. Lett.* **513**, 64–68 (2019).
14. M. Obst, J. J. Dynes, J. R. Lawrence, G. D. W. Swerhone, K. Benzerara, C. Karunakaran, K. Kaznatcheev, T. Tyliszczak, A. P. Hitchcock, Precipitation of amorphous $CaCO_3$ (aragonite-like) by cyanobacteria: A STXM study of the influence of EPS on the nucleation process. *Geochim. Cosmochim. Acta* **73**, 4180–4198 (2009).
15. J. D. Schiffbauer, S. Xiao, Y. Cai, A. F. Wallace, H. Hua, J. Hunter, H. Xu, Y. Peng, A. J. Kaufman, A unifying model for Neoproterozoic–Palaeozoic exceptional fossil preservation through pyritization and carbonaceous compression. *Nat. Commun.* **5**, 5754 (2014).
16. A. Baliński, Y. Sun, Preservation of soft tissue in an Ordovician linguloid brachiopod from China. *Acta Palaeont. Polon.* **58**, 115–120 (2013).
17. J. D. Schiffbauer, T. Selly, S. M. Jacquet, R. A. Merz, L. L. Nelson, M. A. Strange, Y. Cai, E. F. Smith, Discovery of bilaterian-type through-guts in cloudinomorphs from the terminal Ediacaran Period. *Nat. Commun.* **11**, 205 (2020).
18. A. Williams, L. E. Holmer, M. Cusack, Chemico-structure of the organophosphatic shells of siphonotretide brachiopods. *Palaeontology* **47**, 1313–1337 (2004).
19. H. Mukai, K. Terakado, C. G. Reed, in *Microscopic Anatomy of Invertebrates*, F. W. Harrison, R. M. Woollacott, Eds. (Wiley-Liss, 1997), vol. 13, pp. 45–206.
20. A. Williams, in *Microscopic Anatomy of Invertebrates,* F. W. Harrison, R. M. Woollacott, Eds. (Wiley-Liss, 1997), vol. 13, pp. 237–296.
21. C. Garbelli, Shell microstructures in Lopingian brachiopods: Implications for fabric evolution and calcification. *Riv. It. Paleont. Strat.* **123**, 541–560 (2017).
22. M. Jakubowicz, B. Berkowski, M. L. Correa, E. Jarochowska, M. Joachimski, Z. Belka, Stable isotope signatures of middle Palaeozoic ahermatypic rugose corals—Deciphering secondary alteration, vital fractionation effects, and palaeoecological implications. *PLOS ONE* **10**, e0136289 (2015).
23. H. Sun, M. R. Smith, H. Zeng, F. Zhao, G. Li, M. Zhu, Hyoliths with pedicles illuminate the origin of the brachiopod body plan. *Proc. R. Soc. B: Biol. Sci.* **285**, 20181780 (2018).
24. P. D. Taylor, O. Vinn, M. A. Wilson, Evolution of biomineralisation in 'lophophorates'. *Spec. Pap. Palaeont.* **84**, 317–333 (2010).
25. J. A. Cunningham, A. G. Liu, S. Bengtson, P. C. J. Donoghue, The origin of animals: Can molecular clocks and the fossil record be reconciled? *Bioessays* **39**, 1600120 (2017).
26. C. B. Skovsted, G. A. Brock, J. R. Paterson, L. E. Holmer, G. E. Budd, The scleritome of *Eccentrotheca* from the Lower Cambrian of South Australia: Lophophorate affinities and implications for tommotiid phylogeny. *Geology* **36**, 171–174 (2008).
27. Z. Zhang, L. E. Holmer, C. B. Skovsted, G. A. Brock, G. E. Budd, D. Fu, X. Zhang, D. Shu, J. Han, J. Liu, H. Wang, A. Butler, G. Li, A sclerite-bearing stem group entoproct from the early Cambrian and its implications. *Sci. Rep.* **3**, 1066 (2013).
28. S. Conway Morris, A new entoproct-like organism from the Burgess Shale of British Columbia. *Palaeontology* **20**, 833–845 (1977).
29. J. Kimmig, L. C. Strotz, B. S. Liberman, The stalked filter feeder *Siphusauctus lloydguntheri* n. sp. from the middle Cambrian (Series 3, Stage 5) Spence Shale of Utah: Its biological affinities and taphonomy. *J. Paleont* **91**, 902–910 (2018).
30. F. Marlétaz, K. T. C. A. Peijnenburg, T. Goto, N. Satoh, D. S. Rokhsar, A new spiralian phylogeny places the enigmatic arrow worms among gnathiferans. *Curr. Biol.* **29**, 312–318 (2019).
31. G. J. B. Germs, Implications of a sedimentary facies and depositional environmental analysis of the Nama Group in South West Africa/Namibia, in *Evolution of the Damara Orogen of South West Africa/Namibia*, R. M. Miller, Ed. (Geological Society of South Africa Special Publication, 1983), vol. 11, pp. 89–114.
32. R. Wood, S. W. Poulton, A. R. Prave, K.-H. Hoffmann, M. O. Clarkson, R. Guilbaud, J. W. Lyne, R. Tostevin, F. Bowyer, A. M. Penny, A. Curtis, S. A. Kasemann, Dynamic redox

conditions control late Ediacaran metazoan ecosystems in the Nama Group, Namibia. *Precambrian Res.* **261**, 252–271 (2015).
33. J. B. Antcliffe, R. H. T. Calloway, M. D. Brasier, Giving the early fossil record of sponges a squeeze. *Biol. Rev.* **89**, 972–1004 (2014).
34. A. H. Knoll, Biomineralization and evolutionary history. *Rev. Mineral. Geochem.* **54**, 329–356 (2003).
35. H. A. Armstrong, M. D. Brasier, *Microfossils* (Blackwell, ed. 2, 2005).
36. T. N. Taylor, E. L. Taylor, M. Krings, *Paleobotany, The Biology and Evolution of Fossil Plants* (Academic Press/Elsevier, ed. 2, 2009).
37. J. N. A. Hooper, R. W. M. Van Soest, Eds., *Systema Porifera: A Guide to the Classification of Sponges* (Kluwer Academic/Plenum Publishers, 2002).
38. T.-y. Park, J. Woo, D.-J. Lee, D.-C. Lee, S.-b. Lee, Z. Han, S. K. Chough, D. K. Choi, A stem-group cnidarian described from the mid-Cambrian of China and its significance for cnidarian evolution. *Nat. Commun.* **2**, 442 (2011).
39. I. Coronado, A. Pérez-Huerta, S. Rodríguez, Primary biogenic skeletal structures in Multithecopora (Tabulata, Pennsylvanian). *Palaeogeogr. Palaeoclimatol. Palaeoecol.* **386**, 286–299 (2013).
40. T. S. Bagaeva, D. M. Kupaeva, A. A. Vetrova, I. A. Kosevich, Y. A. Kraus, S. V. Kremnyov, cWnt signaling modulation results in a change of the colony architecture in a hydrozoan. *Dev. Biol.* **456**, 145–153 (2019).
41. N. V. Whelan, K. M. Kocot, T. P. Moroz, K. Mukherjee, P. Williams, G. Paulay, L. L. Moroz, K. M. Halanych, Ctenophore relationships and their placement as the sister group to all other animals. *Nat. Ecol. Evol.* **1**, 1737–1746 (2017).
42. A. Williams, C. H. C. Brunton, S. J. Carlson, F. Alvarez, A. D. Ansell, P. G. Baker, M. G. Bassett, R. B. Blodgett, A. J. Boucot, J. L. Carter, L. R. M. Cocks, B. L. Cohen, P. Copper, G. B. Curry, M. Cusack, A. S. Dagys, C. C. Emig, A. B. Gawthrop, R. Gourvennec, R. E. Grant, D. A. T. Harper, L. E. Holmer, H. Hong-fei, M. A. James, J. Yu-gan, J. G. Johnson, J. R. Laurie, S. Lazarev, D. E. Lee, C. Lüter, S. Mackay, D. I. Mac Kinnon, M. O. Manceñido, M. Mergl, E. F. Owen, L. S. Peck, L. E. Popov, P. R. Racheboeuf, M. C. Rhodes, J. R. Richardson, R. Jia-yu, M. Rubel, N. M. Savage, T. N. Smirnova, S. Dong-li, D. Walton, B. Wardlaw, A. D. Wright, *Treatise on Invertebrate Paleontology, Pt H (Revised), Brachiopoda, v. 1* (University of Kansas, Geological Society of America, 1997).
43. A. Kouchinsky, L. E. Holmer, M. Steiner, G. T. Ushatinskaya, The new stem-group brachiopod *Oymurania* from the lower Cambrian of Siberia. *Acta Palaeontol. Polon.* **60**, 963–980 (2014).
44. J. Merkel, B. Lieb, A. Wanniger, Muscular anatomy of an entoproct creeping-type larva reveals extraordinary high complexity and potential shared characters with mollusks. *BMC Evol. Biol.* **15**, 130 (2015).
45. P. D. Taylor, C. Lombardi, S. Cocito, Biomineralization in bryozoans: Present, past and future. *Biol. Rev.* **90**, 1118–1150 (2015).
46. A. O. Borisanova, A new species of solitary Entoprocta, *Loxosomella angusta* sp.n., from the White Sea. *Invertebrate Zoology* **13**, 43–50 (2016).

Acknowledgments: We thank H. Mocke and C. Hoffmann of the Geological Survey of Namibia and the Ministry of Mines and Energy, Namibia. We thank A. Horn and S. Horn of the Omkyk Farm; M. Hall, N. Cayzer, and J. Craven for technical support; and R. Anderson and D. Erwin for useful discussion. **Funding:** A.J.S. acknowledges support from the University of Edinburgh and the International Centre for Carbonate Reservoirs, and R.A.W. acknowledges support from NERC grant (NE/P013651/1). **Author contributions:** A.J.S. conducted the research. R.A.W., A.C., and F.T.B. undertook fieldwork. I.B.B. and A.J.S. conducted the μCT imaging. A.J.S. wrote the first draft of the manuscript, with all authors contributing to the final document. **Competing interests:** The authors declare that they have no competing interests. **Data and materials availability:** All data needed to evaluate the conclusions in the paper are present in the paper and/or the Supplementary Materials. Additional data related to this paper may be requested from the authors.

Submitted 16 October 2020
Accepted 9 November 2020
Published 1 January 2021
10.1126/sciadv.abf2933

Citation: A. J. Shore, R. A. Wood, I. B. Butler, A. Yu. Zhuravlev, S. McMahon, A. Curtis, F. T. Bowyer, Ediacaran metazoan reveals lophotrochozoan affinity and deepens root of Cambrian Explosion. *Sci. Adv.* **7**, eabf2933 (2021).

Ediacaran metazoan reveals lophotrochozoan affinity and deepens root of Cambrian Explosion

A. J. Shore, R. A. Wood, I. B. Butler, A. Yu. Zhuravlev, S. McMahon, A. Curtis and F. T. Bowyer

Sci Adv **7** (1), eabf2933.
DOI: 10.1126/sciadv.abf2933